Particle Accelerators, 1987, Vol. 20, pp. 211–228
0031-2460/87/2004–0211/$20.00/0

Printed in the United States of America

PULSED ION SOURCES FOR ACCELERATION INERTIAL FUSION†

S. HUMPHRIES, JR. and C. BURKHART

Institute for Accelerator and Plasma Beam Technology, University of New Mexico, Albuquerque, New Mexico 87131

(Received November 8, 1985; in final form March 5, 1986)

Experimental results are reported on an extractor for pulsed, high-intensity beams of intermediate-mass ions. Aluminum and indium plasmas were generated using a metal-vapor vacuum arc. A method for electrostatic separation of ions from electrons at the anode was utilized to generate constant current beams, insensitive to plasma flux variations. Electrostatic separation also prevented plasma prefill of the extraction gap, allowing rapid and quiet beam initiation. A maximum extraction voltage of 30 kV was applied across a 1.6-cm gap. Voltage pulse length ranged from 10 to 50 μsec. Peak current densities of 15 mA/cm^2 for Al^+ and In^+ were achieved from an anode with an area of 20 cm^2. Time-of-flight measurements indicated that beam ions were predominantly in the +1 ionization state with no observable species contamination. A divergence measure with a channel-electron-multiplier array implies a normalized emittance of $\epsilon_n < 3 \times 10^{-7} \pi m$ – rad. The technology may have application to the induction linac approach to accelerator inertial fusion.

1. INTRODUCTION

The induction linear ion accelerator approach[1] to Accelerator Inertial Fusion (AIF)[2] places stringent requirements on the plasma source and extraction gap. For near-term experiments with multiple beams,[3] relatively high current densities (10–30 mA/cm^2) of intermediate-mass ions (A = 20–30) are necessary. The area per beam is in the range 10–20 cm^2; proposed configurations have 16 beams. The plasma source must reach an operating equilibrium in a few microseconds and supply plasma for a pulse length of 5–10 μsec. Ideally, there should be no plasma or neutral prefill of high-gradient accelerating structures prior to the extraction pulse. During the pulse, the source must maintain a high degree of spatial and temporal uniformity for good beam optics. Ideally, the extracted beam should be in a single ionization state, since it may be difficult to perform charge-state separation on multiple intense ion beams. The normalized emittance for a 300-mA beam should be less than $\epsilon_n = 4 \times 10^{-7} \pi m$ – rad to satisfy focusing demands.[3]

We have developed novel plasma sources in support of the AIF Injector Project at the Los Alamos National Laboratory (LANL)[4] which meet many of the above requirements. We have concentrated efforts on metal-vapor vacuum arcs.[5] These sources have the following advantages: (i) rapid turn-on, (ii)

† This work was supported by the U.S. Department of Energy under contract No. DE-AC0383-ER13138 and by Los Alamos National Laboratory under contract No. 9X54-K-66711.

simplicity of fabrication and operation, (iii) generation of clean plasmas with little species contamination, (iv) production of a wide variety of ions from metals and semiconductors, and (v) potentially high ion flux. The main drawback of metal-vapor vacuum arcs is that there are substantial temporal variations of plasma flux that would degrade the optics of a conventional extractor. In order to solve this problem, we developed a method of ion extraction based on electrostatic separation of plasma ions from electrons before the plasma reaches the extraction gap.

The principle of the grid-controlled plasma anode is illustrated in Fig. 1. In contrast to conventional extractors with an exposed plasma, two grids are interposed between the plasma source and extraction gap. The plasma grid is maintained at the potential of the plasma source and expansion chamber. This grid references the plasma potential. The extraction gap anode grid is biased to a negative potential with respect to the plasma grid. The potential is high enough to turn all electrons. The result is that only ions can enter the extraction gap. As a consequence, the behavior of the plasma extraction gap anode is identical to that of a thermionic anode. Extracted ion flow is space-charge limited and is therefore

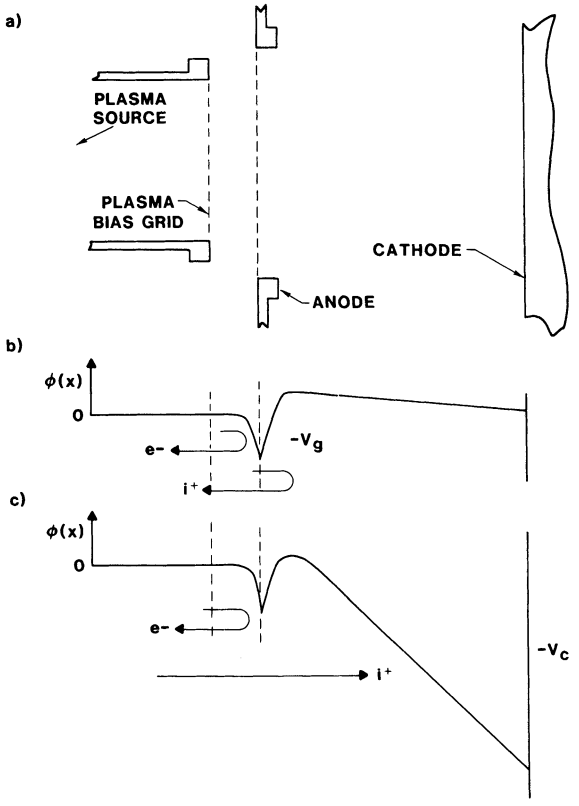

FIGURE 1 Principle of the grid-controlled plasma anode. (a) Grid geometry, (b) particle flow and variation of electrostatic potential with zero extraction voltage, (c) particle flow and variation of electrostatic potential with an applied extraction voltage.

insensitive to the available flux from the plasma source. The beam optics are determined by the shape of the gap anode grid rather than by plasma meniscus effects.[6] The implication is that a well-behaved ion beam can be extracted even if the plasma source properties vary. Figure 1 shows a plot of the potential in the vicinity of the grids for a plasma with finite electron temperature. The plasma potential is positive in the expansion chamber because of electron loss. Ions that flow into the extraction gap in excess of the space-charge limit are forced to réflex at a virtual anode. Because only positive particles can enter the extraction gap, there can be no significant build-up of particles before the extraction voltage is applied.

The physics of grid-controlled ion extraction and initial experiments have been reported elsewhere.[7] In this paper, we report new experimental results on ion beam formation using a pulsed extraction voltage. The parameters of the experiments were chosen to bracket the parameters of the extraction gap of the LANL injector. We have generated pulsed Al^+ beams at current densities up to $15\,mA/cm^2$ in a 1.8-cm gap to 30 kV. The experiments verify space-charge-controlled ion beam extraction, confirm the attainment of equilibrium current densities on a time scale less than 1 μsec, and demonstrate the role of the control grids to prevent plasma prefill of the extraction gap. We also produced beams of In^+ to demonstrate the potential application of metal-vapor vacuum arcs to future heavy-ion fusion experiments. With the pulsed extraction voltage, we were able to perform time-of-flight measurements of beam composition. The measurements showed that the extracted beams had little species contamination and were almost entirely in the +1 ionization state. Local beam-divergence measurements implied an upper limit on normalized emittance of $\epsilon_n = 3 \times 10^{-7} \pi m - \text{rad}$, within the AIF goal for a 300-mA beam.

The experimental apparatus is described in Section 2. Results on extraction of aluminum and indium ions are summarized in Section 3, time-of-flight species measurements are reported in Section 4, and emittance measurements are described in Section 5.

2. EXPERIMENTAL APPARATUS

The experimental system is illustrated in Fig. 2. The vacuum chamber consisted of a 15-cm-diameter Pyrex glass cross. The glass chamber also served as the high-voltage vacuum insulator. The vacuum system was free of hydrocarbons. All insulators were either glass, ceramic, or Teflon. An 8-in. ion pump maintained a vacuum of 5×10^{-6} Torr. The grids were composed of stainless-steel woven mesh (0.0025-cm-diameter wires with 0.025-cm center-to-center spacing). The meshes had a transparency factor of 80%. The electrodes were designed to permit grid replacement. This proved unnecessary; in experiments involving over 1000 pulses, there was no damage to the grids.

The arc source consisted of a stainless-steel anode and a replaceable cathode. The cathode slug was threaded and mounted in a stainless-steel holder. The gap

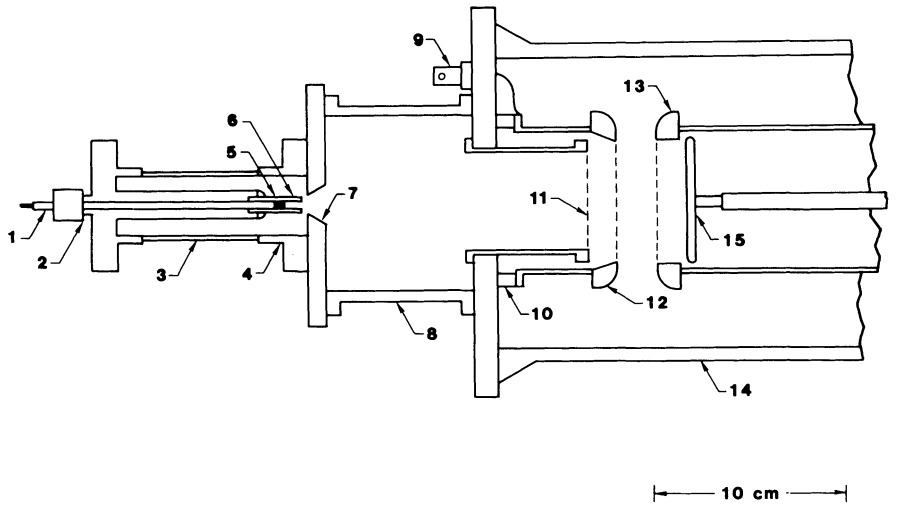

FIGURE 2 Experimental apparatus: 1. Rigid coaxial tubing feedthrough for initiator spark, 2. compression seal, 3. glass insulator, 4. stainless-steel flange, 5. recessed initiator spark, 6. replaceable arc cathode, 7. stainless-steel arc anode, 8. plasma expansion chamber, 9. vacuum feedthrough for anode bias, 10. ceramic standoff, 11. plasma grid, 12. biased extraction-gap anode, 13. extraction-gap cathode, 14. glass vacuum chamber, 15. large-area collector.

was adjusted to approximately 0.08 cm. Larger gaps resulted in the formation of erratic plasmas with high electron temperatures, leading to failure of grid control. Smaller gaps caused reduced flux. The cathode and its support were hollow. A length of rigid coaxial tubing extended the length of the center hole. Following the method developed by Brown,[8] a low-energy vacuum insulator spark on the exposed end of the tubing produced a small amount of plasma to initiate the metal-vapor arc.

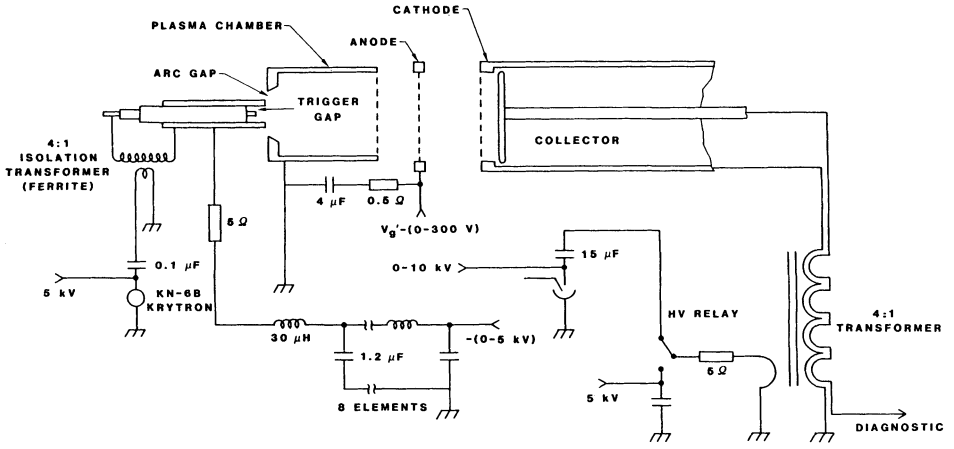

FIGURE 3 Circuit diagram for experimental apparatus. Arc initiator, vacuum arc, anode bias, extraction-gap pulse transformer, transformer reset, and diagnostic isolation arc shown.

The vacuum arc power supply circuit is illustrated in Fig. 3. Arc current was provided by a resistively limited eight-element pulse-forming network. The 5-Ω network was dc charged. The network supplied a constant arc current ranging from 100 to 500 A for a 100-μsec pulse. The trigger discharge was driven by an isolation transformer with 4:1 voltage step-up. The primary voltage on the ferrite core transformer was generated by a 5-kV Krytron circuit. The amount of trigger plasma could be controlled by a variable series resistor in the transformer secondary. Grid bias was supplied by a dc-charged capacitor. A 1-Ω series resistor protected the grid in the event of a short circuit. Ion current drawn by the grid during the plasma pulse was less than 1 A.

The main extraction voltage was provided by a pulse transformer (Fig. 4) designed for ion and electron extraction experiments. The basis of the transformer was a set of three 66-cm-diameter fast-pulse cores composed of 0.005-cm-thick silicon-steel laminations. The three cores had an inner diameter of 30 cm and a thickness of 5 cm, giving a total primary volt-second product of 0.083 V-sec. The cores were linked by a flux-forcing loop to improve the waveform of the magnetically switched voltage pulse. The primary winding consisted of one turn of stripped RG8 high-voltage cable. The winding could be reversed for positive or negative pulses. The secondary consisted of an air-insulated 3.5-turn winding on an insulating standoff. The secondary winding had the following components: a low-resistance copper strap, two 50-Ω diagnostic cables, a 75-Ω 7-kV cable, an ac line, and two 30-Ω 30-kV cables. With the transformer, we had the option to power and control plasma sources with the anode elevated to high voltage or to perform isolated diagnostics with negative high voltage applied to the cathode terminal. In the present experiments, the latter option was used. With careful

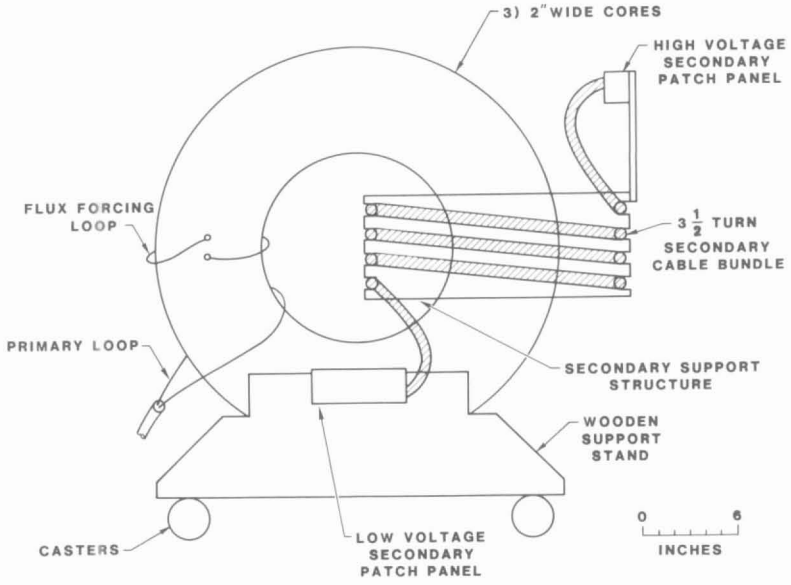

FIGURE 4 Scale drawing of mobile, air-insulated pulse transformer.

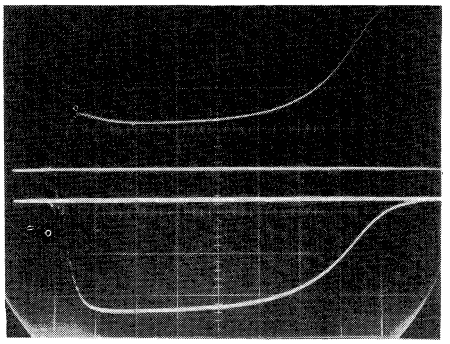

FIGURE 5 Leakage current measurements on 3.5:1 pulse transformer (2-mil silicon-steel laminations, 0.083 V-sec). Top: primary leakage current, 400 A/div; bottom: secondary voltage, open circuit, 9.6 kV/div, 2 μsec/div.

attention to the elimination of ground loops, less than 50 mV of noise was observed with 30 kV of diagnostic isolation on an unshielded oscilloscope 2 m from the high-voltage test stand. The transformer can generate 60-kV pulses. Voltage was limited to 30 kV in the reported experiments because of breakdown on the ungraded vacuum insulator.

The cores were reset by discharge of a 5-kV capacitor through the primary. Reset switching was performed by a high-voltage solenoid relay (Fig. 3). The main pulse was applied from an ignitron-switched 20-kV capacitor. Both the reset and main bank discharged through a 5-Ω series resistor. The output pulse was magnetically switched; the secondary voltage fell to zero when the core volt-second product was reached. A voltage pulse with an open secondary is illustrated in Fig. 5. The upper trace is the primary leakage current, and the lower trace is the secondary voltage. Risetime of the voltage was about 1 μsec.

The properties of the arc plasma were diagnosed in detail in previous experiments.[7,9] Calibrated voltage and current diagnostics were incorporated into the arc source, the grid circuit, and the main extraction gap. Beam diagnostics were performed by electrical probes. Absolute local current-density measurements were performed with the probe illustrated in Fig. 6. The negatively biased ring blocked neutralizing electrons from contributing to the signal. The aperture had a 0.24-cm diameter. At the current densities measured, space-charge expansion of the ion beam in the detector was predicted to be small. An unbiased large-area collector (shown in Fig. 2) was used for relative measurements. The signal cables for the detectors wound through the transformer secondary and were connected to an oscilloscope with 50-Ω terminations.

For time-of-flight measurements, a plate with a 0.3-cm-diameter aperture was added at the cathode, and the collector was withdrawn to a distance of 13 cm from the cathode surface. Measurements of beam angular divergence were performed with a 4-cm channel-electron-multiplier array (CEMA). An aperture plate with four 0.036-cm-diameter holes 0.8 cm from the axis was located at the cathode. The CEMA, 37.2 cm from the aperture plate, amplified the image of the projected beam. The image was transferred directly to photographic film outside

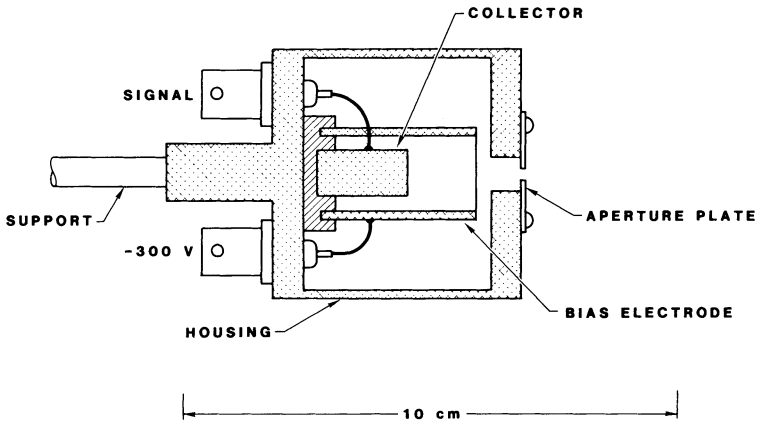

FIGURE 6 Ion current-density probe with biased ring to prevent electron flow.

the vacuum system through a fiber-optic coupler. The reported measurements were time integrated. We have since added circuitry to gate the CEMA for time-resolved measurements.

3. ION EXTRACTION EXPERIMENTS

The arc current and plasma flux for an aluminum plasma-source cathode are shown in Fig. 7. The flux was measured behing the extraction-gap cathode grid with an electrostatic plasma probe biased to ion saturation. There was a delay time of about 20 μsec for the plasma to traverse the 18.5-cm distance to the

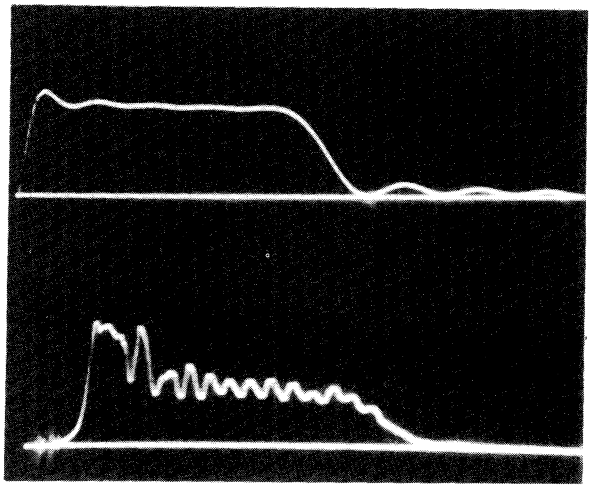

FIGURE 7 Plasma flux measured behind cathode grid with ion-saturation probe, 3-kV charge on PFN. Top: plasma arc driving curent, 200 A/div; bottom: available plasma ion flux, 12.4 mA/cm^2/div, 20 μsec/div.

probe. Figure 7 shows typical behavior for a metal-vapour arc source; there was an initial burst of plasma at start-up, followed by an equilibrium phase with random flux variations on a 5-μsec time scale. Previous measurements[9] on arc plasmas indicated that there was often species contamination during turn-on of systems run at low duty cycle. We found that the species content of the plasma reflected the composition of the cathode at later times when the electrodes were cleared. In the experiments reported here, the application of the extractor voltage was delayed 40 μsec from arc initiation to allow the plasma to reach equilibrium.

We performed experiments to verify that the extractor operated in a space-charge-limited mode when the grid was sufficiently biased. Figure 8 shows results with an aluminum arc cathode. In each pair of traces, the top trace shows the voltage applied to the extraction gap, and the bottom trace shows the signal from the large-area collector. The traces were taken with the same extraction voltage and plasma source properties, but with varying grid voltage. In Fig. 8d, the grid voltage was low. There was a large spike in the collector signal when the extractor voltage was applied. This was caused by plasma prefill of the extraction gap. The signal following start-up was irregular. The extraction gap operated in the source-limited mode; therefore, the extracted current followed random variations in the plasma flux. The flux level was consistent with the measurements of available flux taken with the plasma probe. As the grid voltage was increased (Figs. 8c and 8b), plasma prefill was reduced and the signal became more regular.

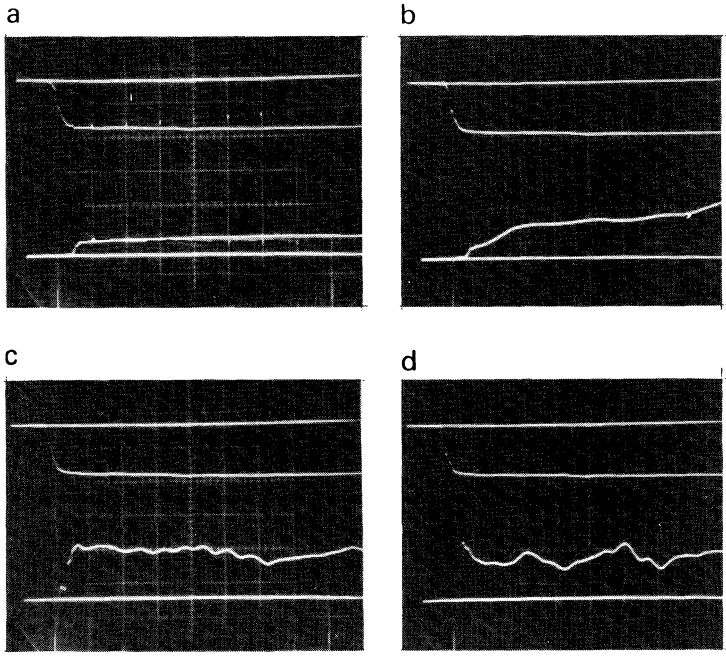

FIGURE 8 Effect of grid voltage on extracted ion current density, aluminum ions. Top: extractor voltage, 4 kV/div; bottom: extracted ion current density, 6.2 mA/cm^2/div, 2 μsec/div. (a) Grid voltage, -100 V; (b) grid voltage, -75V; (c) grid voltage, -50 V; (d) grid voltage, -25 V.

At a grid voltage of −100 V (Fig. 8a), the ion extraction signal reached a constant value at a level well below the source limit. There was no evidence of plasma prefill occurring during the previous 20 μsec of available plasma flux. Furthermore, the flux of high-energy ions was relatively independent of fluctuations in the source. The required grid voltage was in the predicted range. The voltage must be high enough to reduce the thermal electron flux well below the Bohm ion flux. For aluminum ions, the grid must reduce the electron flux by a factor of more than 220. If the electrons have a Maxwellian distribution, the reduction factor for thermal electron flux is approximately $\exp(-eV_g/kT_e)$, where V_g is the magnitude of voltage applied between the plasma source and extraction gap anode and kT_e is the electron temperature. For a 10-eV electron plasma, this translates into grid voltages exceeding 55 V.

Figure 9 shows similar results for an indium plasma. At a low grid voltage, the collector current (top trace) reflects the effect of plasma prefill before application of the voltage. Note the negative signal level before the voltage pulse; this was caused by electron collection from plasma leaking across the extraction gap. In Fig. 9a, there was a gap breakdown associated with plasma prefill. Note further than the flux level in Figs. 9b and 9c had little relationship to the gap voltage. In contrast, at a high grid voltage (Fig. 9d), the ion flux was clearly controlled by the extraction voltage. The small spike at the beginning of the flux signal in Figs. 9c

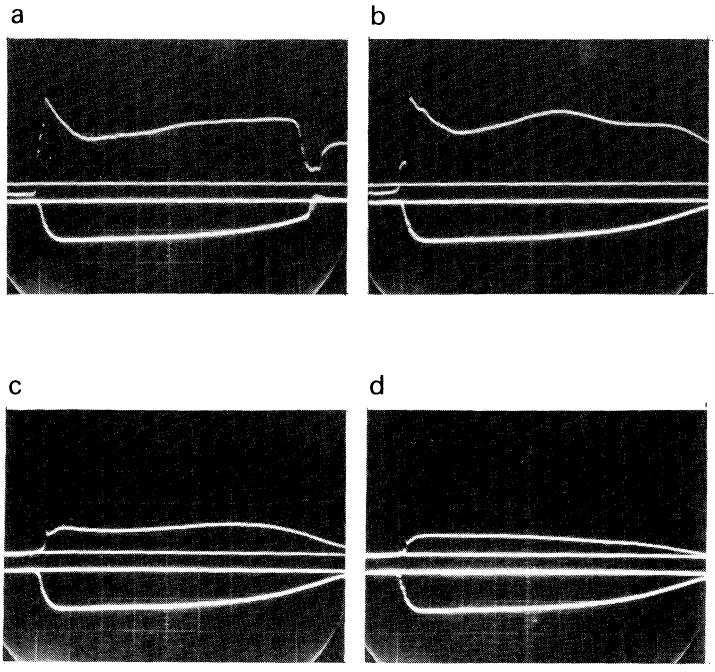

FIGURE 9 Effect of grid voltage on extracted ion current density, indium ions. Top: Net ion current, 200 mA/cm^2/div; bottom: extractor voltage, 10 kV/div. (a) Grid voltage, O V; (b) grid voltage, −50 V; (c) grid voltage, −100 V; (d) grid voltage, −150 V.

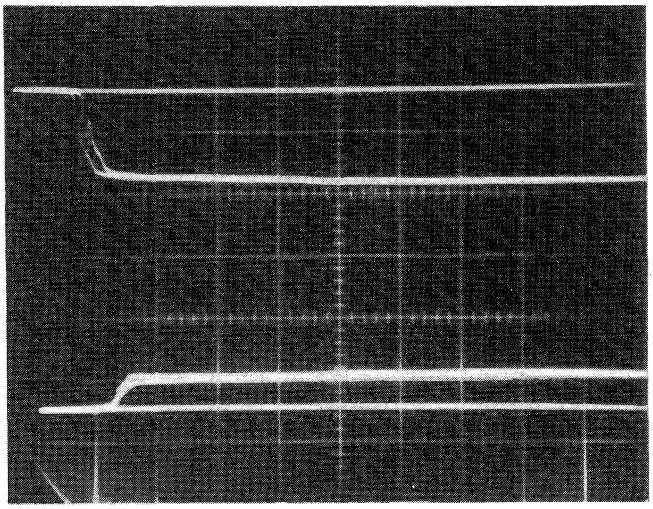

FIGURE 10 Reproducibility of extracted ion current in the space-charge-limited mode, shown by a two-shot overlay; grid voltage, −150 V. Top: extractor voltage, 4 kV/div; bottom: extracted ion current density, 6.2 mA/cm^2/div, 2 μsec/div.

and 9d is a real feature corresponding to velocity bunching of the heavy indium ions traversing the 2-cm distance from the anode to the collector.

Figure 10 shows further evidence that ion flow in the extractor was space-charge limited when the grid voltage was high and when the space-charge-limited flux was well below the available source flux. The figure shows a two-shot overlay of aluminum ion flux for the same extraction voltage. Except for initial effects caused by jitter in applying the transformer voltage, the traces are identical. Control of ion flux by the extractor voltage at high grid voltage is demonstrated in the series of oscillographs of Fig. 11. The properties of the aluminum ion source were maintained constant while the extractor voltage was raised. Note that all oscillographs are two-shot overlays. In the first two traces (Figs. 11a and 11b), the space-charge-limited flux was well below the source limit; hence, the traces are almost identical. When the voltage was raised, the extraction gap flow became comparable to the source flow, and ion, flux reflected random variations in the source flux. At high voltage, the signals became irregular. The traces showed flux irregularities associated with the transition between source-limited and space-charge-limited operation. We have observed this effect previously.[7] We believe that in this circumstance there were large offsets in plasma potential that allowed bursts of plasma to enter the extraction gap.

Measurements of the variation of ion flux with extraction gap voltage are summarized in Fig. 12. The dashed lines are plotted with a slope corresponding to $V^{3/2}$. The ion flux closely follows the space-charge prediction for the 1.8-cm-wide extraction gap. The relative fluxes of indium and aluminum vary by a factor of two at the same voltage, in agreement with space-charge flow predictions.

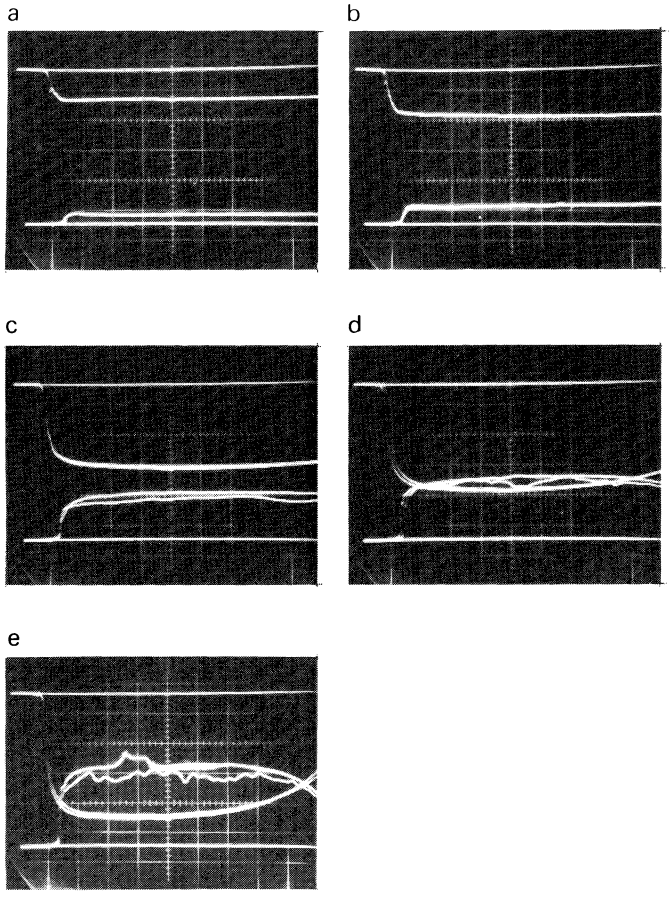

FIGURE 11 Ion current density as a function of extraction voltage, aluminum ions; grid voltage, −150 V. Top: extractor voltage, 4 kV/div; bottom: extracted ion current density, 6.2 mA/cm^2/div, 2 μsec/div. All traces are two-shot overlays.

4. TIME-OF-FLIGHT MEASUREMENTS

The flux of ion beams from a low-energy ion extractor is quite sensitive to variations of injector voltage. This fact, a potential problem associated with linear induction ion accelerators,[10] can be used to advantage for measurements of species in pulsed ion beams. If the rise time of the extractor voltage is comparable to the ion transit time, under most circumstances the arrival time of a particular ion species at a downstream detector is marked by a divergence in the collected current density. The characteristic signature of velocity bunching is useful for identifying species and charge states. Numerical predictions of ion current density 13 cm from the cathode, based on an analytic fit for the transformer voltage

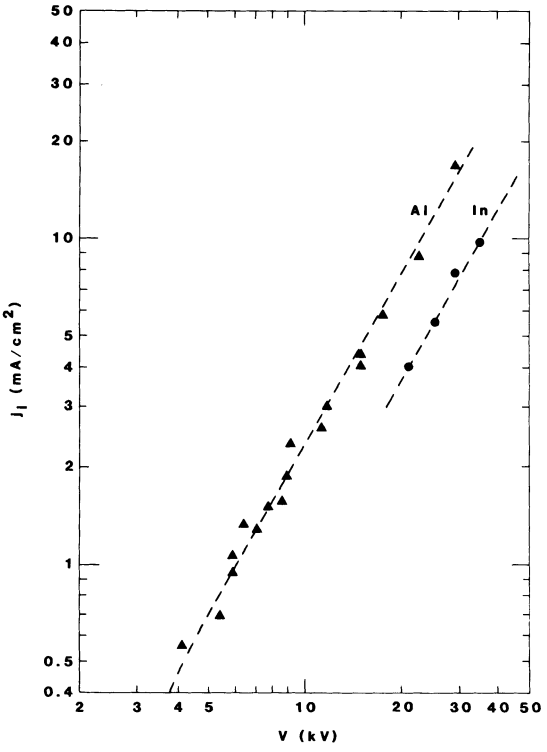

FIGURE 12 Log-log plot of peak ion flux versus extraction gap voltage for Al^+ and In^+, grid voltage, -150 V. Dashed lines have $V^{3/2}$ slope.

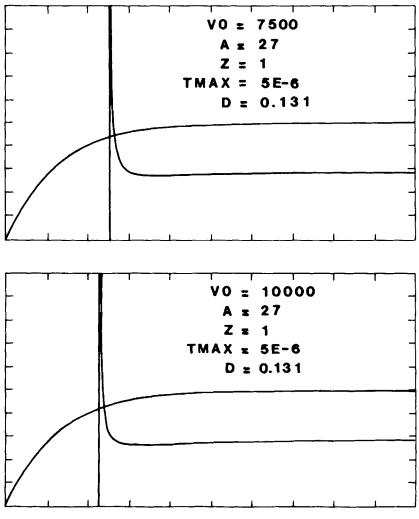

FIGURE 13 Numerical predictions of normalized gap voltage and relative flux of In^+ ions at a detector 13 cm from the extraction gap cathode. Gap transit time effects are not included. Full scale is equal to 5 μsec. (a) Peak voltage, 7500 V; (b) peak voltage, 10,000 V.

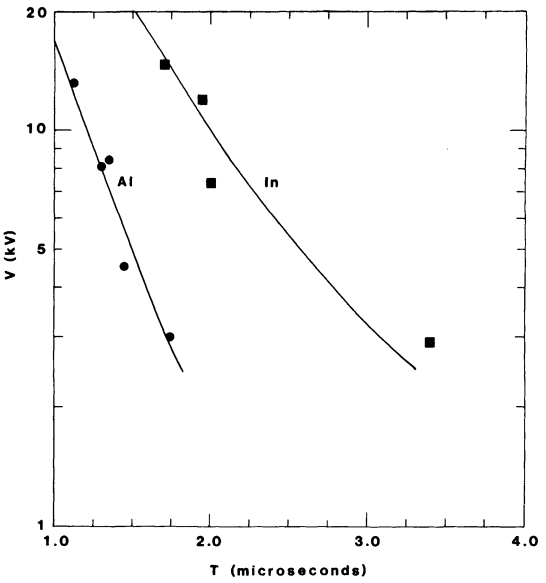

FIGURE 14 Time of flight to a detector 13 cm from extraction gap cathode versus extraction gap voltage for Al^+ and In^+ ions. Circles: measured arrival time, aluminum arc cathode; squares: measured arrival time, indium arc cathode; solid lines: numerical prediction of arrival time.

waveform, are shown in Fig. 13. The graphs correspond to indium at 7.5 keV and 10 keV. A number of runs were combined to generate predictions for the arrival times of In^+ and Al^+, as functions of extraction voltage. These results are plotted as solid lines in the graph of Fig. 14.

Low-energy unneutralized ion beams can be strongly affected by space charge. In order to perform time-of-flight measurements, we added a plate with a small aperture to allow only a small fraction of the beam to propagate into the drift region. The beam flux was reduced to a level where the space-charge potential would not significantly alter the propagation velocity of ions. The net current collected by the probe was small; it was necessary to use a 50-Ω line driver with a 10-kΩ input impedance to get a clean signal. The combination of driver input impedance and probe capacitance limited the signal rise time to 0.3 μsec. Although we could not resolve details of the beam spike, we were able to make good measurements of the arrival time of ions. A typical signal for aluminum ions with the extraction gap operated in the space-charge-limited mode is shown in Fig. 15. The voltage signal is displayed at the top; the time-of-flight probe signal is at the bottom. Note the substantial delay and the clean aluminum signal. The trace indicates that the beam is predominantly Al^+. If doubly ionized aluminum and light-ion contaminants were present, their signals would be separated enough in time to allow easy identification. Note also that, after an initial peak in the signal caused by velocity bunching, that signal is flat. This is another indication that ion flow was space-charge controlled. Not only was the net beam current constant, but also the locally resolved current density at the center of the gap was constant. This implies that the beam was spatially uniform.

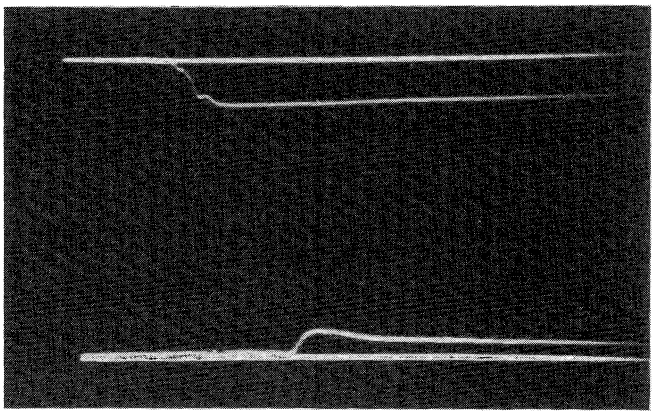

FIGURE 15 Time-of-flight measurement for aluminum ions; distance from cathode mesh to probe, 13 cm. Top: extractor voltage, 4 kV/div; bottom: detector output (uncalibrated), 1 μsec/div.

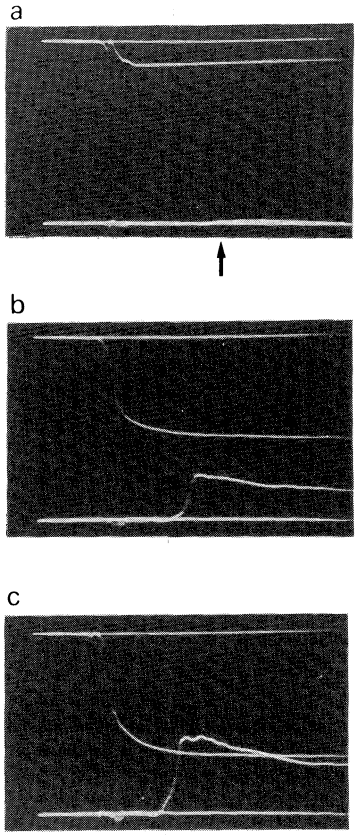

FIGURE 16 Time-of-flight measurement for indium ions; distance from cathode mesh to probe, 13 cm. Top: extractor voltage, 4 kV/div; bottom: detector output (uncalibrated), 1 μsec/div. The arrow on trace (a) indicates the arrival time of ions, identifiable in original oscillograph. (a) peak voltage, 7 kV; (b) peak voltage, 28 kV; (c) peak voltage, 35 kV.

A sequence of time-of-flight traces for indium ions at different values of extraction voltage is given in Fig. 16. Again, note the clean signals and the absence of doubly ionized indium. The signal at low voltage (Fig. 16a) is quite small because of $V^{3/2}$ scaling in the acceleration gap and space-charge expansion in the drift region. The arrival time of ions is identifiable on the original oscillograph of Fig. 16a. The net delay exceeded 1 μsec. Measurements of arrival time for aluminum and indium ions as a function of extractor voltage are summarized in Fig. 14. The measurements are in excellent agreement with numerical predictions. Note that the predictions are absolute, with no adjusted parameters.

The generation of predominantly singly ionized beams from vacuum arcs is an unusual result. Measurements by others[5] indicate a high percentage of multiply charged ions from vacuum arc plasmas. Although we have detected doubly charged aluminum in previous plasma measurements,[9] the percentage is low. Our measurements were taken at a distance from the arc (~10 cm). One possible explanation for the discrepancy is that species filtering occurs in the plasma between the arc and the plasma grid; the plasma potential is predicted from the electron temperature to be about +30–40 V.

5. BEAM DIVERGENCE MEASUREMENTS

We measured the beam divergence using an aperture plate at the cathode and a channel-electron-multiplier array (CEMA) to image the beam projections at a distance of 37.2 cm from the plate. The four apertures were located at a radial distance of 0.8 cm from the system axis in a cross pattern. An on-axis aperture was not included to prevent light from the vacuum arc from reaching the CEMA. The CEMA was carefully light-shielded with reentrant structures to facilitate vacuum pumping. With this precaution, the signal level from diffuse plasma light was well below that of the beam, even in the time-integrated mode.

Typical photographic output of the CEMA assembly is shown in Fig. 17. The data of Fig. 17a were taken with a relatively high voltage between the plasma source and grid (−250 V) and with a high extraction voltage (27 kV). The beams formed well-defined circles with an edge diameter of about 0.7 cm. The pattern of circles was somewhat distorted compared with the pattern on the aperture plate for two reasons: (i) the extractor gap did not have a Pierce geometry, so that there was some space-charge expansion of the beam, and (ii) the extraction gap was mechanically referenced to a commercial Pyrex insulator, so that there were angular and translational errors in aligning the extraction gap cathode and anode. These two factors were confirmed by noting changes in the spot pattern with varying extraction gap voltage and with macroscopic gap alignment. The time-integrated spots had relatively small diameters, indicating a high degree of stability in the plasma extraction surface upstream of the anode mesh.

The effect of space-charge expansion on the beams propagating to the CEMA was estimated using a computer code to solve the complete paraxial ray equation. The area of the apertures was 1×10^{-3} cm^2, giving a current of 15 μA per beam

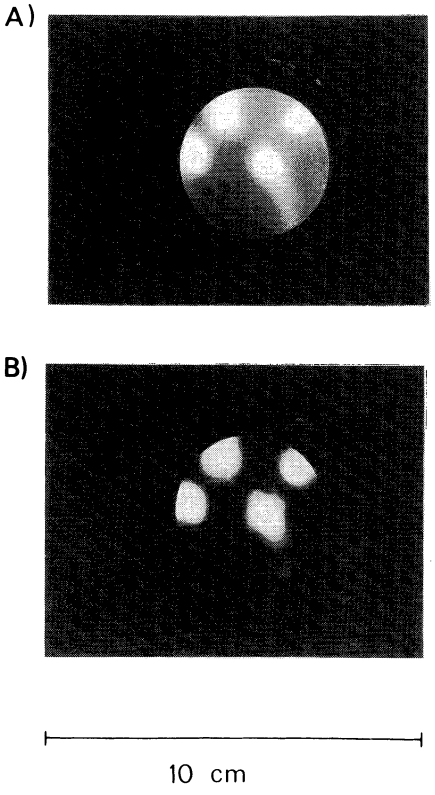

FIGURE 17 Time-integrated photographic output from the CEMA beam-divergence detector, for aluminum ions. The average extraction gap voltage was 27 kV; the current density was 15 mA/cm^2. (a) Voltage between anode grid and plasma source, −250 V; (b) grid voltage, −100 V.

(at 15 mA/cm^2) and a generalized perveance of 10^{-5} (at 27 keV). For a final beam radius of 0.35 cm, the space-charge correction amounted to 30% implying a beam envelope divergence angle of $\Delta r' = 6.7$ mrad. The divergence angle corresponds to a peak ion transverse energy of 1.2 eV. Using this angle to project the beam distribution back across the 1.8-cm extraction gap implies a sampling diameter for each aperture of 0.024 cm, approximately equal to the width of the opening in the anode mesh. Therefore, the measurement was a true indication of beam divergence, averaged over a mesh opening.

If it is assumed that the angular divergence is representative of the distribution across the 5-cm diameter of the active anode (r_0), then the emittance of the extracted beam can be estimated (neglecting nonlinear optical effects in the extraction gap). The normalized emittance is given by

$$\epsilon_n = \beta r_0 \Delta r'. \tag{1}$$

Equation (1) is defined in terms of the boundary of the distribution circumscribing all particles. Substitution into Eq. (1) gives an emittance figure of $3 \times 10^{-7} \pi m$-rad.

We observed that the the emittance exhibited a variation with grid voltage (between the plasma source and gap anode) consistent with the predictions of Ref. 7. Figure 17b shows output from the CEMA detector for the same extractor voltage as Fig. 17a but with the source anode voltage lowered to -100 V. For the plasma density in question, the extraction-sheath width was predicted to be comparable to the mesh spacing, resulting in stronger facet lens focusing and a distorted plasma surface. Note the broadened central spot and the prominent beam halos in Fig. 17b.

In conclusion, the present experiments demonstrate the feasibility of metal-vapor vacuum arcs for application to high-power linear induction ion accelerators. The ion species (Al^+) and current density (15 mA/cm^2) are within the desired range. Present plans for the LANL injector[11] call or an initial gridded beam-control gap operating at a field stress of 8 kV/cm for a 5-μsec pulse. We have shown that gridded extractors can operate well above this limit in the presence of beam for long pulse lengths.

ACKNOWLEDGEMENTS

We would like to thank D. Keefe of the Lawrence Berkeley Laboratory, whose suggestion of the use of electrostatic grids to prevent plasma prefill of extractor gaps provided much of the motivation for this work. We would also like to thank E. Meyer of the Los Alamos National Laboratory for suggesting the design of the electron trap detector. H. Rutkowski, D. Wilson, and K. Riepe of the Los Alamos National Laboratory provided many useful suggestions.

REFERENCES

1. A. Faltens, E. Hoyer, and D. Keefe, in H. J. Doucat and J. M. Buzzi, Eds., *Proc. 4th Interm. Conf. High Power Electron and Ion Beam Research and Tech.* (Ecole Polytechnique, 1981), P. 751, and A. Faltens, E. Hoyer, D. Keefe, and L. J. Laslett, *IEEE Trans. Nucl. Sci.* **NS–26,** 3106 (1979).
2. R. C. Arnold, Ed., *Proc. Heavy Ion Fusion Workshop,* Argonne National Laboratory report ANL–79–41 (1979) and W. B. Herrmannsfeldt, Ed., *Proc. Heavy Ion Fusion Workshop,* Lawrence Berkeley Laboratory report LBL–10301 (1980).
3. D. L. Judd, Ed., *Multiple Beam Experiment (MBE), Conceptual Design and Program Description,* Lawrence Berkeley Laboratory report PUB–5123 (1984).
4. E. O. Ballard, E. A. Meyer, H. L. Ruthkowski, R. P. Shurter, and F. W. Van Haaften, *IEEE Trans. Nucl. Sci.* **NS–32,** 1788 (1985).
5. J. V. R. Herberlein and D. R. Porto, *IEEE Trans. Plasma Sci.* **PS–11,** 152 (1983): R. Adler and S. T. Picraux, to be published in *Nucl. Instrum. Methods Phys. Res.*; I. G. Brown, J. E. Gavin, and R. A. MacGill, to be published in *Appl. Phys. Lett.*; and C. Burkhart, S. Coffey, G. Cooper, S. Humphries, Jr., L. K. Len, A. D. Logan, M. Savage, and D. M. Woodall, *Nucl. Instrum. Methods Phys. Res.* **B10/11,** 792 (1985).
6. See, for instance, C. Lejeune, Extraction of Ion Beams from Plasma Surfaces," in A. Septier, Ed., *Applied Charged Particle Optics-Very-High- Beams* (Academic Press, New York, 1983), p. 207.
7. S. Humphries, Jr., C. Burkhart, L. K. Len, M. Savage, D. M. Woodall, H. Rutkowski, H. Oona, and R. Shurter, to be published in *J. Appl. Phys.*

8. I. G. Brown, *IEEE Trans. Nucl. Sci.* **NS–32,** 1723 (1985).
9. L. K. Len, C. Burkhart, G. Cooper, S. Humphries, Jr., M. Savage, and D. M. Woodall, to be published in *IEEE Trans. Plasma Sci.*
10. S. Humphries, Jr., *J. Appl. Phys.* **51,** 2338 (1980).
11. K. Riepe, Los Alamos National Laboratory, private communication.